Carbon 126 (2018) 271–278

Contents lists available at ScienceDirect

Carbon

journal homepage: www.elsevier.com/locate/carbon

Active modulation of electromagnetically induced transparency analogue in terahertz hybrid metal-graphene metamaterials

Shuyuan Xiao [a], Tao Wang [a, *], Tingting Liu [b], Xicheng Yan [a], Zhong Li [c, d], Chen Xu [e]

[a] Wuhan National Laboratory for Optoelectronics, Huazhong University of Science and Technology, Wuhan 430074, People's Republic of China
[b] School of Electronic Information and Communications, Huazhong University of Science and Technology, Wuhan 430074, People's Republic of China
[c] Center for Materials for Information Technology, The University of Alabama, Tuscaloosa 35487, USA
[d] Department of Physics and Astronomy, The University of Alabama, Tuscaloosa 35487, USA
[e] Department of Physics, New Mexico State University, Las Cruces 88001, USA

ARTICLE INFO

Article history:
Received 17 June 2017
Received in revised form
10 October 2017
Accepted 11 October 2017
Available online 13 October 2017

ABSTRACT

Metamaterial analogues of electromagnetically induced transparency (EIT) have been intensively studied and widely employed for slow light and enhanced nonlinear effects. In particular, the active modulation of the EIT analogue and well-controlled group delay in metamaterials have shown great prospects in optical communication networks. Here we integrate a monolayer graphene into metal-based terahertz (THz) metamaterials, and realize a complete modulation in the resonance strength of the EIT analogue via manipulating the Fermi level of graphene. The physical mechanism lies in the active tuning of the damping rate of the dark mode resonator through the recombination effect of the conductive graphene. This work presents a novel modulation strategy of the EIT analogue in the hybrid metamaterials, and paves the way towards designing very compact slow light devices to meet the future demand of ultrafast optical signal processing.

1. Introduction

Electromagnetically-induced transparency (EIT) refers to the formation of a narrow transparency window within a broad absorption profile upon the application of an indirect excitation and the quantum destructive interference between the two excitation channels in a three-level atomic system[1]. This phenomenon is always accompanied by an extreme modification of the dispersion properties and thus potentially useful in many applications, such as slow light [2–4] and enhanced nonlinear effects [5,6]. However, realizing the conventional quantum EIT requires the stable optical pumping and often cryogenic temperature, whose complexities severely restrict practical applications, especially with respect to on-chip integration. These barriers have been overcome by considering that the underlying physics behind the EIT phenomenon is actually classical, and the analogue behaviors can be reproduced using coupled harmonic oscillators and RLC electric circuits [7,8]. This physical insight leads to the realization of the EIT analogues in a series of classical optical systems, such as coupled microresonators [9,10], photonic crystal waveguides [11,12], a waveguide side-coupled to resonators [13,14] and metamaterials [15–17], which are robust and free from the scathing experimental requirements of quantum optics. In particular, the metamaterial analogues of EIT through the near field coupling between the bright and dark mode resonators, have enabled the realization of this phenomenon at frequencies in radio-frequency (RF) [18–20], terahertz (THz) [21–26], near-infrared [27–29] and visible regimes [30,31] through defining a correspondingly tailored geometry for the unit cell. Due to the subwavelength thickness, these EIT analogues with the accompanying slow light and enhanced nonlinear effects have shown great prospects in designing very compact devices, such as optical filters [32,33], optical buffers [34,35] and ultrasensitive biosensors [36,37].

For practical applications, an active modulation of the EIT analogue and consequently the well-controlled group delay are highly desirable. To this end, an active metamaterial is a superior candidate. Up to now, a variety of strategies have been proposed to actively modulate the EIT analogues in metamaterial devices, such as mechanically reconfigurable metamaterials [38–40], hybrid metamaterials through integrating with photoactive semiconductors [41–44], superconductors [45,46], and phase change media [47–49]. As for hybrid metamaterials, in the

* Corresponding author.
E-mail address: wangtao@hust.edu.cn (T. Wang).

https://doi.org/10.1016/j.carbon.2017.10.035
0008-6223/

milestonework [42] Gu J et al. demonstrated an active control of THz waves in classical EIT metamaterials at room temperature through integrating Silicon (Si) islands into functional unit cells and realized an on-to-off modulation of the EIT analogue by optical pump-terahertz probe (OPTP) measurements. However, the response time in this kind of modulation process is limited by the recovery time of the excited carriers in Si ($\sim$ 1 ms), which severely hinders applications in ultrafast optoelectronics. Graphene, a two-dimensional (2D) material with a plethora of exceptional electronic and photonic properties, has garnered enormous attention [50–52]. The relaxation time of the excited carriers in the monolayer graphene is on the order of picosecond, showing a promising future for ultrafast response [53,54]. Moreover, the conductivity of graphene can also be continuously tuned via manipulating its Fermi level by electric gating or photo-induced doping, which lays the direct foundation for efficient real-time control of resonance in metamaterials [55–63]. In the recent decade, a variety of graphene-based metamaterials have been proposed to realize the EIT analogues, where the nanostructured graphene can support the localized surface plasmon (LSP) resonance and act as the bright and dark mode resonators in the infrared and THz regimes [64–72]. However, on the one hand, it is the resonance frequency rather than the resonance strength of the transparency window will be tuned via manipulating the Fermi level of graphene in this kind of modulation process, therefore an on-to-off modulation of the EIT analogue at the specific resonance frequency without affecting adjacent frequency spectra can not be realized. On the other hand, the nanostructured graphene resonators in the isolated fashion can not be expediently tuned in practice and the ultrasmall feature size that corresponds to resonance entering into the THz gap is also challenging in the nanoscale fabrication. Very recently, the monolayer graphene has been proposed to integrate into the metal-based resonant metamaterials to actively modulate the EIT analogues using its plasmonic response in the infrared and THz regimes, addressing the latter concern to a great degree [73–76]. However, these pioneering works still mainly focus on the active modulation of the resonance frequency rather than the resonance strength of the transparency window, which may introduce additional noises at adjacent frequency spectra in the modulation process.

In the present work, we propose, for the first time to the best of our knowledge, an active modulation of the resonance strength of the EIT analogue in THz resonant metamaterials through integrating a monolayer graphene into the unit cell. The simulation results show that a complete modulation in the resonance strength of the EIT analogue can be realized at the specific resonance frequency without affecting adjacent frequency spectra via manipulating the Fermi level of graphene. The theoretical analysis based on the coupled harmonic oscillator model and distributions of the electric field and surface charge density reveal that the active modulation is attributable to the change in the damping rate of the dark mode resonator by the recombination effect of the conductive graphene. In addition, the well-controlled group delay accompanying EIT is also calculated for slow light applications. The picosecond-order response time of graphene facilitates the ultrafast optical modulation, and the monolayer morphology possesses the advantage of being easier to fabricate and manipulate, showing much better efficiency and feasibility than previous studies. Therefore, this work not only demonstrates the use of graphene in the THz hybrid metamaterials to the active modulation of the EIT analogue, but also paves the way towards designing very compact slow light devices with ultrafast response, which can play a vital role in the future THz communications.

2. The geometric structure and numerical model

The schematic illustration and geometric parameters of our proposed hybrid structure are shown in Fig. 1(a) and (b). Here we employ the classical structure to produce the EIT analogue, similar to [42]. The unit cell of Aluminum (Al)-based resonant metamaterials is arranged in a periodical array with lattice constants of $P_x = 80$ μm and $P_y = 120$ μm, and composed of a cut wire (CW) and a pair of identical but oppositely oriented split ring resonators (SRRs) on the top of a Si substrate. The CW is $L = 85$ μm in length and $W = 5$ μm in width; the SRRs are $l = 29$ μm in side length and $g = 5$ μm in split gap. The coupling distance between the CW and the SRRs is set to $s = 7$ μm. The thickness of both of the resonators is $t_{Al} = 200$ nm and the substrate is assumed to be semi-infinite. The optical properties of Al in the THz regime are described by the Drude model [77]

$$\varepsilon_{Al} = \varepsilon_\infty - \frac{\omega_p^2}{\omega^2 + i\omega\gamma}, \tag{1}$$

where the plasma frequency $\omega_p = 2.24 \times 10^{16}$ rad/s and the damping constant $\gamma = 1.22 \times 10^{14}$ rad/s. The refractive index of Si is taken as $n_{Si} = 3.42$.

The monolayer graphene is placed under the SRRs and can be modeled as a 2D flat sheet [78,79]. The graphene conductivity is derived using the random-phase approximation (RPA) in the local limit, including both the intraband and interband processes [80–82]

$$\begin{aligned}\sigma_g &= \sigma_{intra} + \sigma_{inter} \\ &= \frac{2e^2 k_B T}{\pi\hbar^2}\frac{i}{\omega + i\tau^{-1}}\ln\left[2\cosh\left(\frac{E_F}{2k_B T}\right)\right] + \frac{e^2}{4\hbar}\left[\frac{1}{2}\right. \\ &\quad \left. + \frac{1}{\pi}\arctan\left(\frac{\hbar\omega - 2E_F}{2k_B T}\right) - \frac{i}{2\pi}\ln\frac{(\hbar\omega + 2E_F)^2}{(\hbar\omega - 2E_F)^2 + 4(k_B T)^2}\right],\end{aligned} \tag{2}$$

where e is the charge of an electron, k_B is the Boltzmann constant, T is the operation temperature, $\hbar$ is the reduced Planck's constant, ω is the angular frequency of the incident light, τ is the carrier relaxation time and E_F is the Fermi level.

In the lower THz regime, the contribution originated from the interband process is negligible due to the Pauli exclusion principle when the Fermi level of graphene increases above half of the photon level. Here we only consider highly doped graphene with the Fermi level $E_F \gg k_B T$ and $E_F \gg \hbar\omega$, therefore graphene conductivity can be safely reduced to the Drude-like model [83,84]

$$\sigma_g = \frac{e^2 E_F}{\pi\hbar^2}\frac{i}{\omega + i\tau^{-1}}, \tag{3}$$

where the carrier relaxation time $\tau = (\mu E_F)/(e v_F^2)$ depends on the carrier mobility μ, the Fermi level E_F and the Fermi velocity v_F. Here we employ $\mu = 3000$ cm^2/V•s and $v_F = 1.1 \times 10^6$ m/s throughout the calculations, which are consistent with the experimental measurements [85,86].

As predicted by the equations (2) and (3), the graphene conductivity can be continuously tuned via manipulating its Fermi level. The fabrication and modulation processes follow the steps below [73,74]. Firstly, a monolayer graphene is grown on a copper foil using a chemical vapor deposition (CVD) method and subsequently transferred onto a Si substrate using Marble's reagent solution to remove the copper foil. Secondly, Al-based resonant

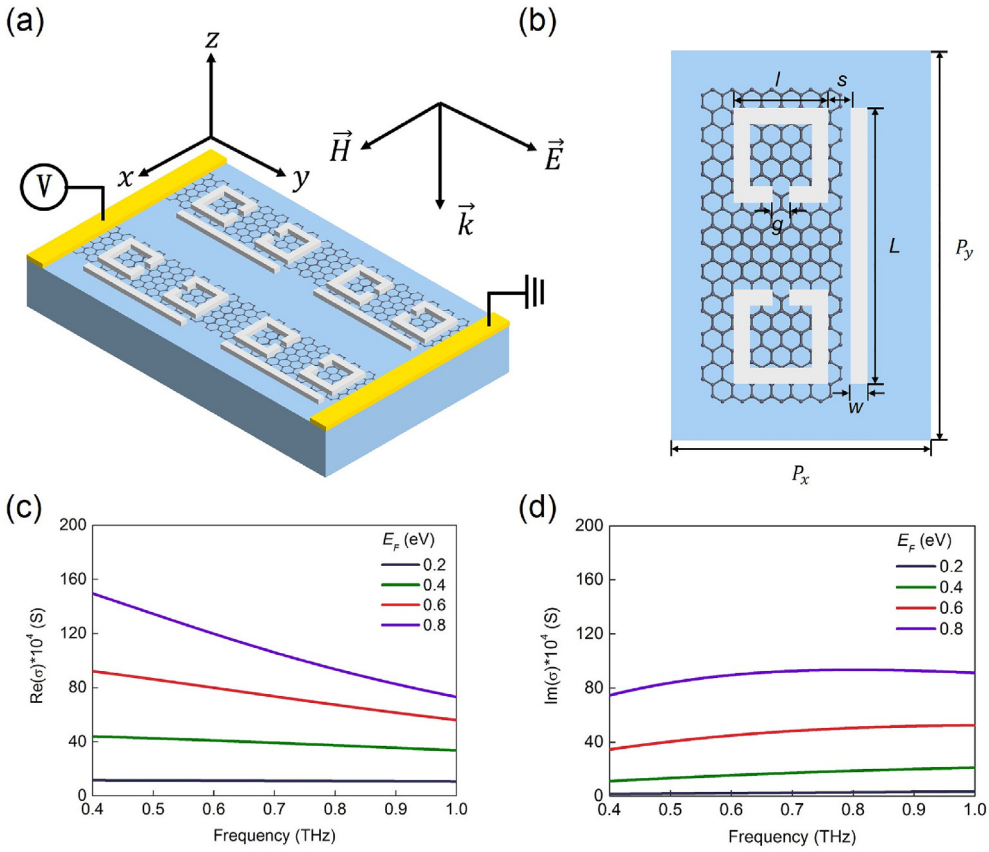

Fig. 1. (a) The schematic illustration of our proposed hybrid metamaterials with a normally incident plane wave. (b) The top view of the unit cell. The geometrical parameters are $L = 85$ μm, $W = 5$ μm, $l = 29$ μm, $g = 5$ μm, $s = 7$ μm, $P_x = 80$ μm and $P_y = 120$ μm, respectively. (c) The real part and (d) the imaginary part of the frequency dependent graphene conductivity. The Fermi level is varied from 0.2 eV to 0.8 eV, as shown in the insets. (A colour version of this figure can be viewed online.)

metamaterials are fabricated on the top of the monolayer graphene using an electron beam lithography (EBL) technique. Finally, a pair of gold (Au) electrodes are deposited on both sides of the monolayer graphene using another EBL step. The electric gating voltage is applied to manipulate the Fermi level of graphene. Consequently, the frequency dependent graphene conductivity at the selected values of the Fermi level are shown in Fig. 1(c) and (d).

The full-wave numerical simulations are performed using the finite-difference time-domain method (FDTD Solutions, Lumerical Inc., Canada). In the calculations, the moderate mesh grid is adopted to balance the simulation time and accuracy. The periodical boundary conditions are employed in the *x* and *y* directions and perfectly matched layers are utilized in the *z* direction along the propagation of the incident plane wave.

3. Simulation results and discussions

In order to investigate the EIT analogue in the Al-based resonant metamaterials, we simulate three sets of arrays with the unit cell composed of a CW, a pair of SRRs and both of them, respectively, and the corresponding transmission spectra are shown in Fig. 2. The CW exhibits a typical LSP resonance mode at 0.65 THz, which is the basic and direct response of metamaterials to the incident plane wave and possesses a broad resonance line width caused by the strong radiative losses. However, the SRRs that can support an LC resonance mode with a narrow line width at the very similar frequency (not shown) do not respond to this excitation due to the reserved structural symmetry with respect to the polarization of the incident plane wave. When both of the CW and the SRRs are

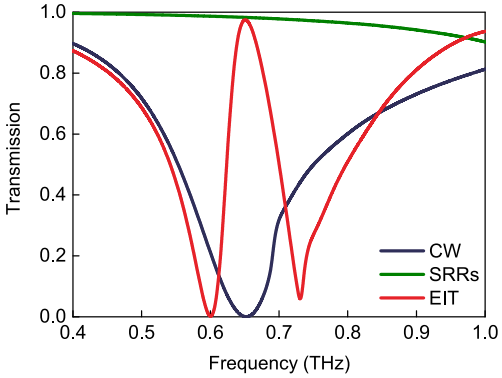

Fig. 2. The simulated transmission spectra of the CW, the SRRs and the EIT metamaterials. (A colour version of this figure can be viewed online.)

simultaneously arranged into the unit cell, a narrow transparency window is clearly observed within a broad absorption profile at 0.65 THz. In this configuration, the CW that can be directly excited by the incident plane wave acts as a bright mode resonator, and the SRRs that can not be directly excited by this excitation act as a dark mode resonator. The near field coupling between them leads to an indirect excitation of the LC resonance mode in the SRRs and the classical destructive interference between the LSP and LC resonance modes gives rise to an EIT analogue.

We also plot the electric field and surface charge density distributions at the resonance frequency to further illuminate the

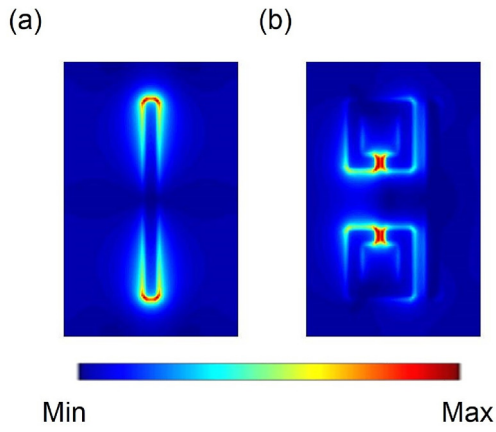

Fig. 3. The simulated electric field distributions of (a) the CW and (b) the EIT metamaterials at 0.65 THz. (A colour version of this figure can be viewed online.)

underlying physics behind the EIT analogue. As shown in Fig. 3(a), before coupling with the SRRs, the CW is directly excited by the incident plane wave with a very strong enhancement of the electric field concentrating on the edges and corners, and correspondingly in Fig. 4(a), a symmetric distribution of the opposite charges along the CW can be nicely observed and the net induced dipoles show a clear tendency to follow the polarization of the incidence plane wave. These distributions correspond to the LSP resonance mode in the CW and validate its function as the bright mode resonator. After the SRRs arranged into the unit cell, however, the strong electric field enhancement entirely transfers to the vicinity of the splits through the near field coupling with the CW in Fig. 3(b), and a large amount of the opposite charges accumulate at two ends of each split, indicating obvious circulation distributions of the surface charge density along SRRs and making them as magnetic dipoles in Fig. 4(b). These are characteristic behaviors of the LC resonance mode, which demonstrate this dark resonance mode in the SRRs is indirectly excited by coupling with the CW. Because the strength of the indirect excitation is comparable to that of the direct excitation but with a π phase difference [15,87], the LSP and LC resonance modes interfere destructively with each other, thus giving rise to the narrow transparency window. Note that the electric field in the CW is almost completely suppressed, which validates the destructive interference at the transparency peak.

Next, we integrate a monolayer graphene into the unit cell and investigate its modulation effect on the EIT analogue in the Al-

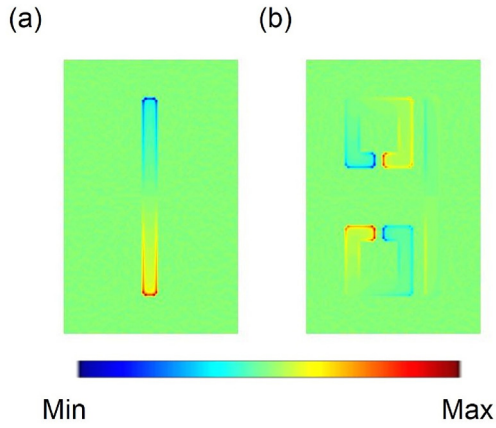

Fig. 4. The simulated surface charge density distributions of (a) the CW and (b) the EIT metamaterials at 0.65 THz. (A colour version of this figure can be viewed online.)

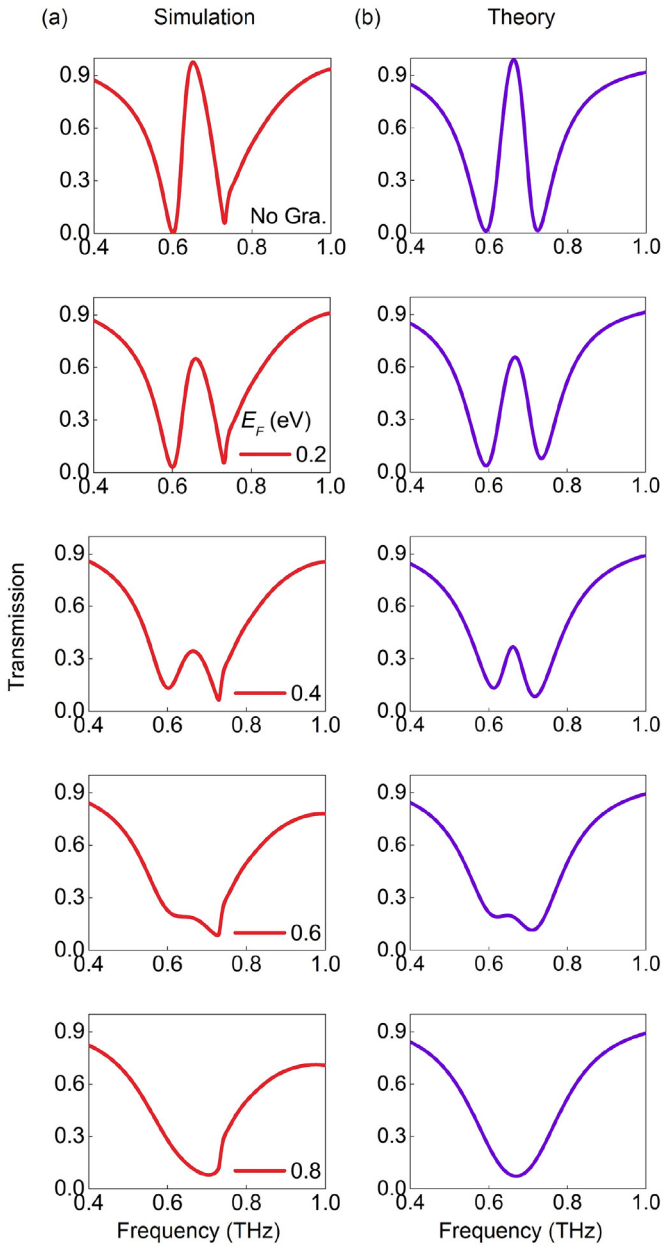

Fig. 5. (a) The simulated transmission spectra of the hybrid metamaterials with the increasing of the Fermi level of graphene. (b) The corresponding analytical fitted transmission spectra with the increasing of the damping rate of the dark mode resonator. (A colour version of this figure can be viewed online.)

based resonant metamaterials. As shown in Fig. 5(a), in the presence of the monolayer graphene under the SRRs, the EIT analogue undergoes a great change in the resonance strength, leading to an on-to-off modulation at the specific resonance frequency without affecting adjacent frequency spectra with the increasing of the Fermi level of graphene. To quantitatively characterize this induced change in the resonance strength, we introduce the reduction degree in the transmission as $\Delta T = (T_0 - T_g) \times 100\%$, where T_0 and T_g refer to transmissions at the transparency peak of the EIT analogue without and with the monolayer graphene, respectively. When the Fermi level starts at 0.2 eV, the transparency peak has an obvious decline from the initial value, and the reduction degree in the transmission is $\Delta T = 33\%$. As E_F gradually increases to 0.4 eV, the transparency peak continues to fall and ΔT goes up to 63%. Then

when E_F comes to 0.6 eV, the transparency peak begins to disappear and ΔT grows to as much as 78%. Finally, with the maximum Fermi level of 0.8 eV, the narrow transparency window merges into the broad absorption profile and only a LSP-like resonance remains with $\Delta T = 84\%$, thus obtaining a complete modulation in the resonance strength of the EIT analogue. Here, we would like to highlight that graphene used in the active modulation is in the monolayer morphology rather than the isolated fashion, which is easier to fabricate and manipulate. Besides, the on-to-off modulation of the EIT analogue requires only a Fermi level of 0.8 eV, which has already been accessed by electric gating experimentally [88–90]. Therefore, the active modulation of the EIT analogue in our proposed hybrid metamaterials shows much better efficiency and feasibility than previous studies.

In order to reveal the physical mechanism of the active modulation of the EIT analogue, we employ the coupled harmonic oscillator model to quantitatively describe the near field coupling between the bright and dark mode resonators in our proposed hybrid metamaterials. To mimic the quantum EIT in a three-level atomic system, this simple model includes a ground state $|0\rangle$ and two excited states $|1\rangle$ and $|2\rangle$. $|0\rangle \rightarrow |1\rangle$ defines the dipole-allowed transition, corresponding to the LSP bright resonance mode in the CW; $|0\rangle \rightarrow |2\rangle$ defines the dipole-forbidden transition, corresponding to the LC dark resonance mode in the SRRs. Besides, the transition between $|1\rangle$ and $|2\rangle$ corresponds to the near field coupling between the CW and the SRRs, which therefore introduces the destructive interference between two possible excitation channels: $|0\rangle \rightarrow |1\rangle$ and $|0\rangle \rightarrow |1\rangle \rightarrow |2\rangle \rightarrow |1\rangle$, leading to the cancellation of absorption at the EIT frequency. The interference in the metamaterials can be analytically described by the coupled differential equations [15,17]

$$\ddot{x}_1 + \gamma_1 \dot{x}_1 + \omega_0^2 x_1 + \kappa x_2 = E, \tag{4}$$

$$\ddot{x}_2 + \gamma_2 \dot{x}_2 + (\omega_0 + \delta)^2 x_2 + \kappa x_1 = 0, \tag{5}$$

where x_1, x_2, γ_1 and γ_2 are the resonance amplitudes and the damping rates of the bright and dark mode resonators, respectively, ω_0 is the resonance frequency of the bright mode resonator before coupling with the dark mode resonator, δ is the detuning of the resonance frequency of the dark mode resonator from the bright mode resonator, and κ denotes the coupling coefficient between the two resonators. After solving the coupled equations (4) and (5) with the approximation $\omega - \omega_0 \ll \omega_0$, we obtain the susceptibility χ of the EIT metamaterials [66,69]

$$\chi = \chi_r + i\chi_i \propto \frac{(\omega - \omega_0 - \delta) + i\frac{\gamma_2}{2}}{\left(\omega - \omega_0 + i\frac{\gamma_1}{2}\right)\left(\omega - \omega_0 - \delta + i\frac{\gamma_2}{2}\right) - \frac{\kappa^2}{4}}. \tag{6}$$

Note that the energy dissipation is proportional to the imaginary part χ_i, therefore the transmission T can be calculated through $T = 1 - g\chi_i$, where g is the geometric parameter indicating the coupling strength of the bright mode resonator with the incident electric field E.

As shown in Fig. 5(b), we present the analytical fitted transmission spectra according to the coupled harmonic oscillator model, which exhibit a very good agreement with the simulation results. The corresponding fitting parameters as a function of the Fermi level of graphene are listed in Fig. 6. In the modulation process, γ_1, δ and κ stay roughly constant with the increasing of E_F, however, the damping rate of the dark mode resonator γ_2 increases by more than two orders of magnitude. Therefore, the theoretical model indicates that the active modulation is attributable to the change in the damping rate of the dark mode resonator. In our

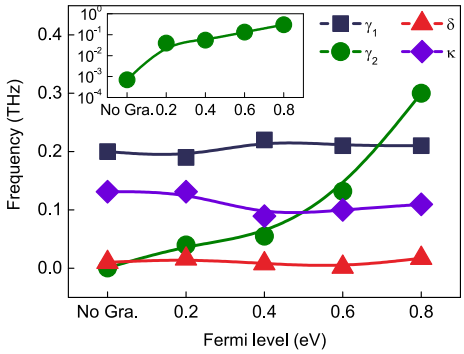

Fig. 6. The fitting parameters γ_1, γ_2, δ and κ as a function of the Fermi level of graphene. The unit of κ is THz^2. (A colour version of this figure can be viewed online.)

proposed hybrid metamaterials, the monolayer graphene behaves like a quasi-metal with the high conductivity, and once placed under the SRRs, it connects the two ends of each split, enhances the losses in the SRRs and thus weakens the destructive interference between the bright and dark resonance modes. With the maximum Fermi level of 0.8 eV, the losses become too large to sustain the dark resonance mode in the SRRs, which consequently leads to the disappearance of the transparency peak at the EIT frequency.

Here we plot the electric field and surface charge density distributions at the resonance frequency to further substantiate the physical mechanism of the active modulation of the EIT analogue. Without the monolayer graphene, the LC resonance mode in the SRRs is indirectly excited by coupling with the CW and in reverse interference destructively with the LSP resonance mode in the CW at the EIT frequency, which reflects in the distributions is the transfer of the strong electric field enhancement from the CW to the SRRs and the accumulation of the opposite charges at two ends of each split, as repeated in Figs. 7(a) and 8(a). In this configuration, the SRRs exhibit very small damping rate. With the monolayer graphene placed under the SRRs, the opposite charges are recombined and neutralized through this conductive layer, which leads to a strong suppression of the electric field enhancement in the SRRs. This is demonstrated in Figs. 7(b) and 8(b), when the Fermi level of graphene gradually increases to 0.4 eV, the electric field is redistributed, where the enhancement in the SRRs significantly declines while that in the CW obviously increases, and correspondingly, the opposite charges become much slighter in the SRRs and the induced dipoles along the CW begin to reappear. With the maximum Fermi level of 0.8 eV, the recombination effect of the monolayer graphene can be more pronounced with the higher conductivity. As shown in Figs. 7(c) and 8(c), the opposite charges are almost completely neutralized, and consequently the electric

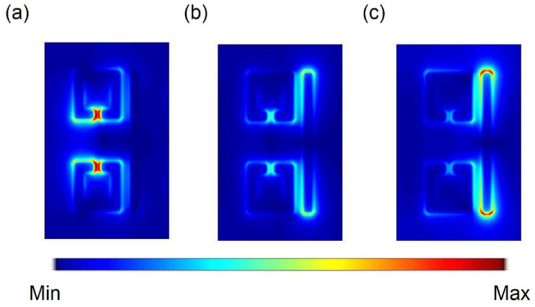

Fig. 7. The simulated electric field distributions of the EIT metamaterials at 0.65 THz. The corresponding Fermi levels of graphene are (a) No Gra, (b) 0.4 eV, (c) 0.8 eV. (A colour version of this figure can be viewed online.)

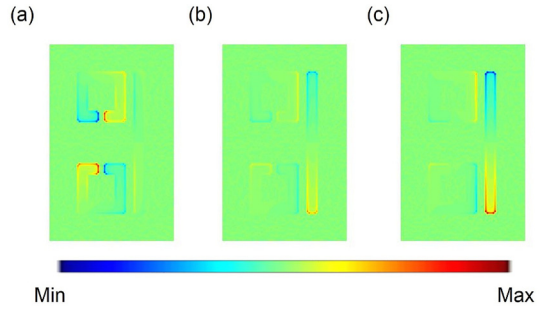

Fig. 8. The simulated surface charge density distributions of the EIT metamaterials at 0.65 THz. The corresponding Fermi levels of graphene are (a) No Gra, (b) 0.4 eV, (c) 0.8 eV. (A colour version of this figure can be viewed online.)

field enhancement in the SRRs is nearly eliminated and that in the CW is fully recovered as before coupling with the SRRs. The SRRs exhibit too large damping rate to support the LC resonance mode, and therefore the destructive interference between the LSP and LC resonance modes disappears.

As mentioned above, the EIT phenomenon is always accompanied by the extreme modification of the dispersion properties, which leads to slow light effect. Here we introduce the group delay t_g to describe the slow light capability, which is expressed as [14]

$$t_g = \frac{d\psi}{d\omega}, \tag{7}$$

where ψ is the transmission phase shift. In comparison with the conventionally used group refractive index n_g, the calculation of t_g does not require the effective thickness of the hybrid metamaterials, which is difficult to define due to the semi-infinite substrate, and more importantly, t_g is directly related to the practical applications of slow light devices. As shown in Fig. 9(a) and (b), we calculate the transmission phase shift and group delay of the hybrid metamaterials. Without the monolayer graphene, the phase slope is positive and steepest within the transparency window, leading to the largest group delay of 5.72 ps, which corresponds to the group delay of a 1.72-mm distance of free space propagation. With the monolayer graphene placed under the SRRs, the hybrid metamaterials gradually lose the slow light capability with the increasing of the Fermi level. With the maximum Fermi level of 0.8 eV, the group delay characteristics of EIT completely turn into those of LSP-like resonance. The well-controlled group delay in our proposed hybrid metamaterials is comparable to previous studies [42,43], and can be strategically important in designing very compact slow light devices with ultrafast response.

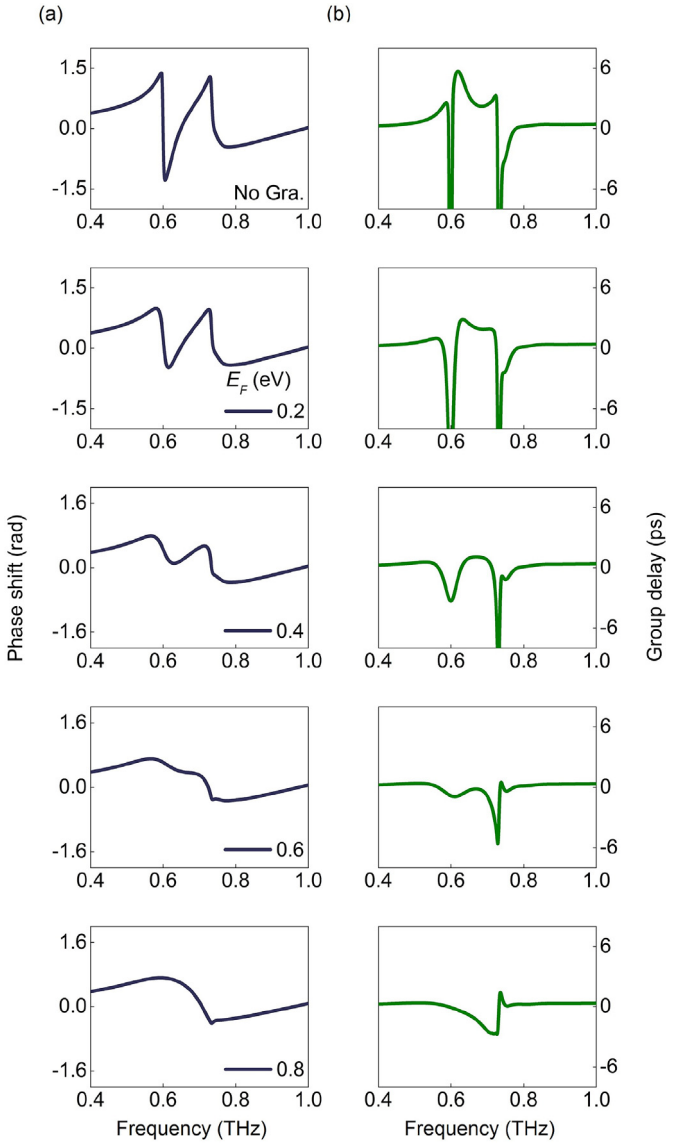

Fig. 9. (a) The simulated transmission phase shift and (b) group delay of the EIT metamaterials with the increasing of the Fermi level of graphene. (A colour version of this figure can be viewed online.)

4. Conclusions

To conclude, we have realized an active modulation of the resonance strength of the EIT analogue through integrating a monolayer graphene into the THz resonant metamaterials. The FDTD simulation results show that an on-to-off modulation in the resonance strength of the EIT analogue can be completed at the specific resonance frequency without affecting adjacent frequency spectra with the maximum Fermi level of 0.8 eV. We employ the coupled harmonic oscillator model to describe the near field coupling in the hybrid metamaterials that agrees very well with the simulation results, and the theoretical analysis reveals that the active modulation is attributable to the change in the damping rate of the dark mode resonator. The electric field and surface charge density distributions further illuminate that the physical mechanism lies in the recombination effect of the conductive graphene. In addition, the well-controlled group delay is also calculated for slow light applications. The active modulation of the EIT analogue in our proposed hybrid metal-graphene metamaterials creates great possibilities for designing very compact slow light devices that can find potential applications in THz communication networks.

Acknowledgments

The author Shuyuan Xiao (SYXIAO) expresses his deepest gratitude to his Ph.D. advisor Tao Wang for providing guidance during this project. SYXIAO would also like to thank Dr. Qi Lin, Dr. Guidong Liu, Dr. Shengxuan Xia (Hunan University) and Dr. Quan Li (Tianjin University) for beneficial discussions on graphene optical properties. This work is supported by the National Natural Science Foundation of China (Grant No. 61775064, 61376055, 61006045 and 11647122), the Fundamental Research Funds for the Central Universities (HUST: 2016YXMS024) and the Project of Hubei Provincial Department of Education (Grant No. B2016178).

References

[1] S.E. Harris, Electromagnetically induced transparency, Phys. Today 50 (7) (1997) 36–42.
[2] L.V. Hau, S.E. Harris, Z. Dutton, C.H. Behroozi, Light speed reduction to 17 metres per second in an ultracold atomic gas, Nature 397 (6720) (1999) 594–598.
[3] M. Lukin, A. Imamoğlu, Controlling photons using electromagnetically induced transparency, Nature 413 (6853) (2001) 273–276.
[4] I. Novikova, R.L. Walsworth, Y. Xiao, Electromagnetically induced transparency-based slow and stored light in warm atoms, Laser & Photonics Rev. 6 (3) (2012) 333–353.
[5] H. Schmidt, A. Imamoglu, Giant kerr nonlinearities obtained by electromagnetically induced transparency, Opt. Lett. 21 (23) (1996) 1936–1938.
[6] Y. Zhang, A.W. Brown, M. Xiao, Opening four-wave mixing and six-wave mixing channels via dual electromagnetically induced transparency windows, Phys. Rev. Lett. 99 (12) (2007) 123603.
[7] C. Garrido Alzar, M. Martinez, P. Nussenzveig, Classical analog of electromagnetically induced transparency, Am. J. Phys. 70 (1) (2002) 37–41.
[8] J. Souza, L. Cabral, R. Oliveira, C. Villas-Boas, Electromagnetically-induced-transparency-related phenomena and their mechanical analogs, Phys. Rev. A 92 (2) (2015) 023818.
[9] D.D. Smith, H. Chang, K.A. Fuller, A. Rosenberger, R.W. Boyd, Coupled-resonator-induced transparency, Phys. Rev. A 69 (6) (2004) 063804.
[10] Q. Xu, S. Sandhu, M.L. Povinelli, J. Shakya, S. Fan, M. Lipson, Experimental realization of an on-chip all-optical analogue to electromagnetically induced transparency, Phys. Rev. Lett. 96 (12) (2006) 123901.
[11] S.F. Mingaleev, A.E. Miroshnichenko, Y.S. Kivshar, Coupled-resonator-induced reflection in photonic-crystal waveguide structures, Opt. Express 16 (15) (2008) 11647–11659.
[12] X. Yang, M. Yu, D.L. Kwong, C.W. Wong, All-optical analog to electromagnetically induced transparency in multiple coupled photonic crystal cavities, Phys. Rev. Lett. 102 (17) (2009) 173902.
[13] M.F. Yanik, W. Suh, Z. Wang, S. Fan, Stopping light in a waveguide with an all-optical analog of electromagnetically induced transparency, Phys. Rev. Lett. 93 (23) (2004) 233903.
[14] H. Lu, X. Liu, D. Mao, Plasmonic analog of electromagnetically induced transparency in multi-nanoresonator-coupled waveguide systems, Phys. Rev. A 85 (5) (2012) 053803.
[15] S. Zhang, D.A. Genov, Y. Wang, M. Liu, X. Zhang, Plasmon-induced transparency in metamaterials, Phys. Rev. Lett. 101 (4) (2008) 047401.
[16] N. Papasimakis, V.A. Fedotov, N. Zheludev, S. Prosvirnin, Metamaterial analog of electromagnetically induced transparency, Phys. Rev. Lett. 101 (25) (2008) 253903.
[17] N. Liu, L. Langguth, T. Weiss, J. Kästel, M. Fleischhauer, T. Pfau, et al., Plasmonic analogue of electromagnetically induced transparency at the drude damping limit, Nat. Mater. 8 (9) (2009) 758–762.
[18] P. Tassin, L. Zhang, R. Zhao, A. Jain, T. Koschny, C.M. Soukoulis, Electromagnetically induced transparency and absorption in metamaterials: the radiating two-oscillator model and its experimental confirmation, Phys. Rev. Lett. 109 (18) (2012) 187401.
[19] S. Han, R. Singh, L. Cong, H. Yang, Engineering the fano resonance and electromagnetically induced transparency in near-field coupled bright and dark metamaterial, J. Phys. D. Appl. Phys. 48 (3) (2014) 035104.
[20] L. Zhu, F.Y. Meng, L. Dong, Q. Wu, B.J. Che, J. Gao, et al., Magnetic metamaterial analog of electromagnetically induced transparency and absorption, J. Appl. Phys. 117 (17) (2015) 17D146.
[21] R. Singh, C. Rockstuhl, F. Lederer, W. Zhang, Coupling between a dark and a bright eigenmode in a terahertz metamaterial, Phys. Rev. B 79 (8) (2009) 085111.
[22] R. Singh, I.A. Al-Naib, M. Koch, W. Zhang, Sharp fano resonances in thz metamaterials, Opt. Express 19 (7) (2011) 6312–6319.
[23] R. Singh, I.A. Al-Naib, Y. Yang, D. Roy Chowdhury, W. Cao, C. Rockstuhl, et al., Observing metamaterial induced transparency in individual fano resonators with broken symmetry, Appl. Phys. Lett. 99 (20) (2011) 201107.
[24] X. Liu, J. Gu, R. Singh, Y. Ma, J. Zhu, Z. Tian, et al., Electromagnetically induced transparency in terahertz plasmonic metamaterials via dual excitation pathways of the dark mode, Appl. Phys. Lett. 100 (13) (2012) 131101.
[25] Z. Zhu, X. Yang, J. Gu, J. Jiang, W. Yue, Z. Tian, et al., Broadband plasmon induced transparency in terahertz metamaterials, Nanotechnology 24 (21) (2013) 214003.
[26] M. Manjappa, S.P. Turaga, Y.K. Srivastava, A.A. Bettiol, R. Singh, Magnetic annihilation of the dark mode in a strongly coupled bright–dark terahertz metamaterial, Opt. Lett. 42 (11) (2017) 2106–2109.
[27] G.Y. Si, E.S.P. Leong, W. Pan, C.C. Chum, Y.J. Liu, Plasmon-induced transparency in coupled triangle-rod arrays, Nanotechnology 26 (2) (2014) 025201.
[28] Y. Yang, Kravchenko II, D.P. Briggs, J. Valentine, All-dielectric metasurface analogue of electromagnetically induced transparency, Nat. Commun. 5 (2014) 5753.
[29] J. Chen, R. Xu, P. Mao, Y. Zhang, Y. Liu, C. Tang, et al., Realization of fanolike resonance due to diffraction coupling of localized surface plasmon resonances in embedded nanoantenna arrays, Plasmonics 10 (2) (2015) 341–346.
[30] S. Biswas, J. Duan, D. Nepal, K. Park, R. Pachter, R.A. Vaia, Plasmon-induced transparency in the visible region via self-assembled gold nanorod heterodimers, Nano Lett. 13 (12) (2013) 6287–6291.
[31] J. Yan, P. Liu, Z. Lin, H. Wang, H. Chen, C. Wang, et al., Directional fano resonance in a silicon nanosphere dimer, ACS Nano 9 (3) (2015) 2968–2980.
[32] S. Hu, H. Yang, S. Han, X. Huang, B. Xiao, Tailoring dual-band electromagnetically induced transparency in planar metamaterials, J. Appl. Phys. 117 (4) (2015) 043107.
[33] Z. Cheng, L. Chen, X. Zang, B. Cai, Y. Peng, Y. Zhu, Ultrathin dual-mode filtering characteristics of terahertz metamaterials with electrically unconnected and connected u-shaped resonators array, Opt. Commun. 342 (2015) 20–25.
[34] T. Nakanishi, T. Otani, Y. Tamayama, M. Kitano, Storage of electromagnetic waves in a metamaterial that mimics electromagnetically induced transparency, Phys. Rev. B 87 (16) (2013) 161110.
[35] J. Wang, B. Yuan, C. Fan, J. He, P. Ding, Q. Xue, et al., A novel planar metamaterial design for electromagnetically induced transparency and slow light, Opt. Express 21 (21) (2013) 25159–25166.
[36] N. Liu, T. Weiss, M. Mesch, L. Langguth, U. Eigenthaler, M. Hirscher, et al., Planar metamaterial analogue of electromagnetically induced transparency for plasmonic sensing, Nano Lett. 10 (4) (2009) 1103–1107.
[37] G.D. Liu, X. Zhai, L.L. Wang, Q. Lin, S.X. Xia, X. Luo, et al., A high-performance refractive index sensor based on fano resonance in si split-ring metasurface, Plasmonics (2017) 1–5, https://doi.org/10.1007/s11468-016-0478-9.
[38] P. Pitchappa, M. Manjappa, P.H. Chong, R. Singh, N. Singh, C. Lee, Active control of electromagnetically induced transparency analog in terahertz mems metamaterial (advanced optical materials 4/2016), Adv. Opt. Mater. 4 (4) (2016) 541–547.
[39] P. Pitchappa, M. Manjappa, P.H. Chong, Y. Qian, R. Singh, N. Singh, et al., Active control of near-field coupling in conductively coupled micro-electromechanical system metamaterial devices, Appl. Phys. Lett. 108 (11) (2016) 977.
[40] P. Pitchappa, M. Manjappa, P.H. Chong, R. Singh, N. Singh, C. Lee, Active control of electromagnetically induced transparency with dual dark mode excitation pathways using mems based tri-atomic metamolecules, Appl. Phys. Lett. 109 (21) (2016) 211103.
[41] H.T. Chen, J.F. O'hara, A.K. Azad, A.J. Taylor, R.D. Averitt, D.B. Shrekenhamer, et al., Experimental demonstration of frequency-agile terahertz metamaterials, Nat. Photonics 2 (5) (2008) 295–298.
[42] J. Gu, R. Singh, X. Liu, X. Zhang, Y. Ma, S. Zhang, et al., Active control of electromagnetically induced transparency analogue in terahertz metamaterials, Nat. Commun. 3 (2012) 1151.
[43] Q. Xu, X. Su, C. Ouyang, N. Xu, W. Cao, Y. Zhang, et al., Frequency-agile electromagnetically induced transparency analogue in terahertz metamaterials, Opt. Lett. 41 (19) (2016) 4562–4565.
[44] M. Manjappa, Y.K. Srivastava, L. Cong, I. Al-Naib, R. Singh, Active photoswitching of sharp fano resonances in thz metadevices, Adv. Mater 29 (3) (2017) 1603355.
[45] B.B. Jin, J.B. Wu, C.H. Zhang, X.Q. Jia, T. Jia, L. Kang, et al., Enhanced slow light in superconducting electromagnetically induced transparency metamaterials, Supercond. Sci. Technol. 26 (7) (2013) 074004.
[46] W. Cao, R. Singh, C. Zhang, J. Han, Plasmon-induced transparency in metamaterials: active near field coupling between bright superconducting and dark metallic mode resonators, Appl. Phys. Lett. 103 (10) (2013) 917.
[47] M.J. Dicken, K. Aydin, I.M. Pryce, L.A. Sweatlock, E.M. Boyd, S. Walavalkar, et al., Frequency tunable near-infrared metamaterials based on vo2 phase transition, Opt. Express 17 (20) (2009) 18330–18339.
[48] Z.L. Samson, K.F. Macdonald, F. De Angelis, B. Gholipour, K. Knight, C.C. Huang, et al., Metamaterial electro-optic switch of nanoscale thickness, Appl. Phys. Lett. 96 (14) (2010) 551.
[49] S. Wang, L. Kang, D.H. Werner, Hybrid resonators and highly tunable terahertz metamaterials enabled by vanadium dioxide (vo2), Sci. Rep. 7 (1) (2017) 4326.
[50] K.S. Novoselov, A.K. Geim, S.V. Morozov, D. Jiang, Y. Zhang, S.V. Dubonos, et al., Electric field effect in atomically thin carbon films, Science 306 (5696) (2004) 666–669.
[51] F. Bonaccorso, Z. Sun, T. Hasan, A. Ferrari, Graphene photonics and optoelectronics, Nat. Photonics 4 (9) (2010) 611–622.
[52] Q. Li, L. Cong, R. Singh, N. Xu, W. Cao, X. Zhang, et al., Monolayer graphene sensing enabled by the strong fano-resonant metasurface, Nanoscale 8 (39) (2016) 17278–17284.
[53] K.J. Yee, J.H. Kim, M.H. Jung, B.H. Hong, K.J. Kong, Ultrafast modulation of optical transitions in monolayer and multilayer graphene, Carbon 49 (14) (2011) 4781–4785.
[54] W. Li, B. Chen, C. Meng, W. Fang, Y. Xiao, X. Li, et al., Ultrafast all-optical graphene modulator, Nano Lett. 14 (2) (2014) 955–959.
[55] L. Ju, B. Geng, J. Horng, C. Girit, M. Martin, Z. Hao, et al., Graphene plasmonics for tunable terahertz metamaterials, Nat. Nanotechnol. 6 (10) (2011) 630–634.
[56] J. Li, Y. Zhou, B. Quan, X. Pan, X. Xu, Z. Ren, et al., Graphene–metamaterial hybridization for enhanced terahertz response, Carbon 78 (2014) 102–112.
[57] X. He, Z.Y. Zhao, W. Shi, Graphene-supported tunable near-ir metamaterials, Opt. Lett. 40 (2) (2015) 178–181.
[58] X. He, Tunable terahertz graphene metamaterials, Carbon 82 (2015) 229–237.
[59] Q. Li, Z. Tian, X. Zhang, N. Xu, R. Singh, J. Gu, et al., Dual control of active graphene–silicon hybrid metamaterial devices, Carbon 90 (2015) 146–153.
[60] Y. Fan, N.H. Shen, T. Koschny, C.M. Soukoulis, Tunable terahertz meta-surface with graphene cut-wires, ACS Photonics 2 (1) (2015) 151–156.
[61] Y. Fan, N.H. Shen, F. Zhang, Z. Wei, H. Li, Q. Zhao, et al., Electrically tunable

goos–hänchen effect with graphene in the terahertz regime, Adv. Opt. Mater. 4 (11) (2016) 1824–1828.
[62] J.D. Kim, Y.G. Lee, Graphene-based plasmonic tweezers, Carbon 103 (2016) 281–290.
[63] J. Linder, K. Halterman, Graphene-based extremely wide-angle tunable metamaterial absorber, Sci. Rep. 6 (2016) 31225.
[64] X. Shi, D. Han, Y. Dai, Z. Yu, Y. Sun, H. Chen, et al., Plasmonic analog of electromagnetically induced transparency in nanostructure graphene, Opt. Express 21 (23) (2013) 28438–28443.
[65] H. Cheng, S. Chen, P. Yu, X. Duan, B. Xie, J. Tian, Dynamically tunable plasmonically induced transparency in periodically patterned graphene nanostrips, Appl. Phys. Lett. 103 (20) (2013) 203112.
[66] J. Ding, B. Arigong, H. Ren, M. Zhou, J. Shao, M. Lu, et al., Tuneable complementary metamaterial structures based on graphene for single and multiple transparency windows, Sci. Rep. 4 (2014) 6128.
[67] J. Jiang, Q. Zhang, Q. Ma, S. Yan, F. Wu, X. He, Dynamically tunable electromagnetically induced reflection in terahertz complementary graphene metamaterials, Opt. Mater. Express 5 (9) (2015) 1962.
[68] G. Yao, F. Ling, J. Yue, Q. Luo, J. Yao, Dynamically tunable graphene plasmon-induced transparency in the terahertz region, J. Light. Technol. 34 (16) (2016) 3937–3942.
[69] W. Luo, W. Cai, Y. Xiang, L. Wang, M. Ren, X. Zhang, et al., Flexible modulation of plasmon-induced transparency in a strongly coupled graphene grating-sheet system, Opt. Express 24 (6) (2016) 5784–5793.
[70] X. Zhao, C. Yuan, L. Zhu, J. Yao, Graphene-based tunable terahertz plasmon-induced transparency metamaterial, Nanoscale 8 (33) (2016) 15273–15280.
[71] S.X. Xia, X. Zhai, L.L. Wang, B. Sun, J.Q. Liu, S.C. Wen, Dynamically tunable plasmonically induced transparency in sinusoidally curved and planar graphene layers, Opt. Express 24 (16) (2016) 17886–17899.
[72] X. He, F. Lin, F. Liu, W. Shi, Terahertz tunable graphene fano resonance, Nanotechnology 27 (48) (2016) 485202.
[73] S.H. Mousavi, I. Kholmanov, K.B. Alici, D. Purtseladze, N. Arju, K. Tatar, et al., Inductive tuning of fano-resonant metasurfaces using plasmonic response of graphene in the mid-infrared, Nano Lett. 13 (3) (2013) 1111–1117.
[74] N. Dabidian, I. Kholmanov, A.B. Khanikaev, K. Tatar, S. Trendafilov, S.H. Mousavi, et al., Electrical switching of infrared light using graphene integration with plasmonic fano resonant metasurfaces, Acs Photonics 2 (2) (2015) 216–227.
[75] C. Sun, Z. Dong, J. Si, X. Deng, Independently tunable dual-band plasmonically induced transparency based on hybrid metal-graphene metamaterials at mid-infrared frequencies, Opt. Express 25 (2) (2017) 1242–1250.
[76] Z. Dong, C. Sun, J. Si, X. Deng, Tunable polarization-independent plasmonically induced transparency based on metal-graphene metasurface, Opt. Express 25 (11) (2017) 12251–12259.
[77] M.A. Ordal, R.J. Bell, R.W. Alexander, L.L. Long, M.R. Querry, Optical properties of fourteen metals in the infrared and far infrared: Al, co, cu, au, fe, pb, mo, ni, pd, pt, ag, ti, v, and w, Appl. Opt. 24 (24) (1985) 4493–4499.
[78] M. Merano, Fresnel coefficients of a two-dimensional atomic crystal, Phys. Rev. A 93 (1) (2016) 013832.
[79] J. Linder, K. Halterman, Dynamical tuning between nearly perfect reflection, absorption, and transmission of light via graphene/dielectric structures, Sci. Rep. 6 (2016) 38141.
[80] J. Zhang, C. Guo, K. Liu, Z. Zhu, W. Ye, X. Yuan, et al., Coherent perfect absorption and transparency in a nanostructured graphene film, Opt. Express 22 (10) (2014) 12524–12532.
[81] J. Zhang, Z. Zhu, W. Liu, X. Yuan, S. Qin, Towards photodetection with high efficiency and tunable spectral selectivity: graphene plasmonics for light trapping and absorption engineering, Nanoscale 7 (32) (2015) 13530–13536.
[82] J. Zhang, W. Liu, Z. Zhu, X. Yuan, S. Qin, Towards nano-optical tweezers with graphene plasmons: numerical investigation of trapping 10-nm particles with mid-infrared light, Sci. Rep. 6 (2016) 38086.
[83] S. Xiao, T. Wang, Y. Liu, C. Xu, X. Han, X. Yan, Tunable light trapping and absorption enhancement with graphene ring arrays, Phys. Chem. Chem. Phys. 18 (38) (2016) 26661–26669.
[84] S. Xiao, T. Wang, X. Jiang, X. Yan, L. Cheng, B. Wang, et al., Strong interaction between graphene layer and fano resonance in terahertz metamaterials, J. Phys. D. Appl. Phys. 50 (19) (2017) 195101.
[85] Y. Zhang, Y.W. Tan, H.L. Stormer, P. Kim, Experimental observation of the quantum hall effect and berry's phase in graphene, Nature 438 (7065) (2005) 201–204.
[86] G. Jnawali, Y. Rao, H. Yan, T.F. Heinz, Observation of a transient decrease in terahertz conductivity of single-layer graphene induced by ultrafast optical excitation, Nano Lett. 13 (2) (2013) 524–530.
[87] Z. Ye, S. Zhang, Y. Wang, Y.S. Park, T. Zentgraf, G. Bartal, et al., Mapping the near-field dynamics in plasmon-induced transparency, Phys. Rev. B 86 (15) (2012) 155148.
[88] Z. Fang, S. Thongrattanasiri, A. Schlather, Z. Liu, L. Ma, Y. Wang, et al., Gated tunability and hybridization of localized plasmons in nanostructured graphene, ACS Nano 7 (3) (2013) 2388–2395.
[89] Z. Fang, Y. Wang, A.E. Schlather, Z. Liu, P.M. Ajayan, F.J. Garcia de Abajo, et al., Active tunable absorption enhancement with graphene nanodisk arrays, Nano Lett. 14 (1) (2013) 299–304.
[90] H. Hu, F. Zhai, D. Hu, Z. Li, B. Bai, X. Yang, et al., Broadly tunable graphene plasmons using an ion-gel top gate with low control voltage, Nanoscale 7 (46) (2015) 19493–19500.